

## Opportunities and challenges in GaN metal organic chemical vapor deposition for electron devices

This content has been downloaded from IOPscience. Please scroll down to see the full text.

2016 Jpn. J. Appl. Phys. 55 05FK04

(<http://iopscience.iop.org/1347-4065/55/5S/05FK04>)

View [the table of contents for this issue](#), or go to the [journal homepage](#) for more

Download details:

IP Address: 133.68.98.143

This content was downloaded on 01/09/2017 at 08:51

Please note that [terms and conditions apply](#).

You may also be interested in:

[Criteria for versatile GaN MOVPE tool: high growth rate GaN by atmospheric pressure growth](#)

Koh Matsumoto, Kazutada Ikenaga, Jun Yamamoto et al.

[Molecular beam epitaxy for high-performance Ga-face GaN electron devices](#)

Stephen W Kaun, Man Hoi Wong, Umesh K Mishra et al.

[Recent progress in metal-organic chemical vapor deposition of \(0001\) N-polar group-III nitrides](#)

Stacia Keller, Haoran Li, Matthew Laurent et al.

[Influence of AlN buffer layer thickness on material and electrical properties of InAlN/GaN](#)

[high-electron-mobility transistors](#)

Wei-Ching Huang, Kuan-Shin Liu, Yuen-Yee Wong et al.

[Influence of the carbon-doping location on the material and electrical properties of a AlGaIn/GaN](#)

[heterostructure on Si substrate](#)

Yiqiang Ni, Deqiu Zhou, Zijun Chen et al.

[Hydride-vapor-phase epitaxial growth of highly pure GaN layers with smooth as-grown surfaces on freestanding GaN substrates](#)

Hajime Fujikura, Taichiro Konno, Takehiro Yoshida et al.

[Effects of initial GaN growth mode on the material and electrical properties of AlGaIn/GaN](#)

[high-electron-mobility transistors](#)

Yuen-Yee Wong, Edward Yi Chang, Wei-Ching Huang et al.

[Reduction in Buffer Leakage Current with Mn-Doped GaN Buffer Layer Grown by Metal Organic Chemical Vapor Deposition](#)

Taiki Yamamoto, Hiroyuki Sazawa, Naohiro Nishikawa et al.



## Opportunities and challenges in GaN metal organic chemical vapor deposition for electron devices

Koh Matsumoto<sup>1\*</sup>, Yuya Yamaoka<sup>2</sup>, Akinori Ubukata<sup>2</sup>, Tadanobu Arimura<sup>2</sup>, Guanxi Piao<sup>2</sup>, Yoshiaki Yano<sup>2</sup>, Hiroki Tokunaga<sup>2</sup>, and Toshiya Tabuchi<sup>2</sup>

<sup>1</sup>*GI CS division, TAIYO NIPPON SANZO, Shinagawa, Tokyo 142-8558, Japan*

<sup>2</sup>*Tsukuba Laboratories, TAIYO NIPPON SANZO, Tsukuba, Ibaraki 300-2611, Japan*

\*E-mail: Kou.Matsumoto@tn-sanso.co.jp

Received December 14, 2015; accepted January 25, 2016; published online April 12, 2016

The current situation and next challenge in GaN metal organic chemical vapor deposition (MOCVD) for electron devices of both GaN on Si and GaN on GaN are presented. We have examined the possibility of increasing the growth rate of GaN on 200-mm-diameter Si by using a multiwafer production MOCVD machine, in which the vapor phase parasitic reaction is well controlled. The impact of a high-growth-rate strained-layer-superlattice (SLS) buffer layer is presented in terms of material properties. An SLS growth rate of as high as 3.46  $\mu\text{m}/\text{h}$ , which was 73% higher than the current optimum, was demonstrated. As a result, comparable material properties were obtained. Next, a typical result of GaN doped with Si of  $1 \times 10^{16} \text{cm}^{-3}$  grown at the growth rate of 3.7  $\mu\text{m}/\text{h}$  is shown. For high-voltage application, we need a thick high-purity GaN drift layer with a low carbon concentration, of less than  $10^{16} \text{cm}^{-3}$ . It is shown that achieving a high growth rate by precise control of the vapor phase reaction is still challenge in GaN MOCVD. © 2016 The Japan Society of Applied Physics

### 1. Introduction

GaN metal organic chemical vapor deposition (MOCVD) has made dramatic progress over the past 25 years.<sup>1,2)</sup> While the industrial production technology of blue LEDs on sapphire seems to have reached maturity, GaN also has much potential for application to electron devices owing to its high-breakdown-voltage and large electron mobility.<sup>3,4)</sup> Recently, GaN electron devices grown on 150 mm and 200-mm-diameter silicon substrates have been reported.<sup>5–10)</sup> Although heteroepitaxial growth has been the dominant technology in GaN application, even a GaN electron device on a bulk GaN substrate has been reported with good performance as well as reliability.<sup>11,12)</sup>

We expect that GaN will be deployed in various advanced applications in the future owing to its potential for energy saving. However, to this end, it is important to have a long-term cost reduction road map. Today, the cost reduction model, which is based on increases in wafer size and reactor scale, is going to hit a wall. For the breakthrough in productivity, we recollect the history of the Si-LSI industry. In Si-LSI fabrication, the wafer process was based on a multiwafer batch process until the wafer diameter became 200 mm in the early 1990s. However, when the wafer diameter reached 200 mm, the process was almost completely shifted to a single-wafer process using a cluster configuration, which was initiated by Applied Materials in 1987.<sup>13)</sup> For precision process control, an average control of multiple wafers using a batch was not good enough. Full automated wafer handling was also much easier using a single-wafer process tool than a multiwafer tool. This transition of the production system was enabled by the high process speed of Si LSI technology. Therefore, to trail Si LSI technology, we need to increase the growth rate of nitrides. Since the reactor scale has been increased twice every 4 years until recently, we need to increase the growth rate by a factor of three to keep the same scale-up trend from a 200 mm multiwafer tool to a single 300-mm-diameter wafer cluster tool.<sup>14)</sup> A 200 mm single-wafer cluster tool with a three times higher growth rate has an equivalent throughput to a 200 mm  $\times$  6 multiwafer batch

reactor. In this estimation of the throughput, it is assumed that the peripheral loss time related to temperature ramping, evacuation, and wafer exchange for a multiwafer machine with a low level of automation is nearly 2 h or 40% of the total process time of 5 h for a HEMT on Si. The loss time would be eliminated by a proper combination and sequential process design of the single-wafer multiple-reactor cluster tool.

Firstly, in an attempt of studying the feasibility of a single-wafer process in GaN on Si, we will present the impact of the high-growth-rate strained-layer-superlattice (SLS) buffer layer structure in terms of material properties. We have examined growth rates as high as 3.46  $\mu\text{m}/\text{h}$  for an AlGaIn/GaN HEMT on a 200 mm Si substrate, which is 73% higher than our current optimum condition. As a preliminary result, comparable material properties were obtained. However, we still need to increase the growth rate by another 73% to keep the present pace of productivity improvement. To this end, we need to control the parasitic reaction between trimethylaluminum (TMA) and  $\text{NH}_3$ .<sup>15–17)</sup> Another important issue is carbon control in three orders of concentration.<sup>18)</sup> The carbon concentration was controlled from  $10^{19}$  to  $10^{16} \text{cm}^{-3}$  by varying the growth pressure from 13 to 90 kPa.<sup>23)</sup> To vary growth pressure up to a value near atmospheric pressure, it is important to control the parasitic reaction of the by-product of trimethylgallium and  $\text{NH}_3$ .

Next, we will present a prospective material property, which is required for application in a high-voltage vertical electron device on a GaN substrate. A typical result of GaN doped with Si of  $10^{16} \text{cm}^{-3}$  is shown.<sup>19)</sup> For high-voltage application, we need a thick high-purity GaN drift layer with a very low carbon concentration of less than  $10^{16} \text{cm}^{-3}$ . In addition to high purity, we need a much higher growth rate up to 30  $\mu\text{m}/\text{h}$ . These are the next challenges in GaN MOCVD.

### 2. Experimental method

For growth on a 200 mm (111) Si substrate, a high-growth-rate multiwafer production machine with a capacity of 200 mm  $\times$  6 (TAIYO NIPPON SANZO UR-26k) was used.<sup>20,21)</sup> This reactor can also grow 150 mm  $\times$  10 wafers by using

another wafer holder. The reactor configuration and growth conditions are described in detail in a previous paper.<sup>20,21)</sup> The growth pressure for AlN and AlGaIn was 13 kPa, and the V/III ratios were 900 and 2,000, respectively. The growth pressures for GaN were 13 kPa for the high-carbon-doped layer and 90 kPa for the low-carbon-doped layer. The V/III ratios for GaN growth were 650 and 1,800 for the current optimum conditions and 360 and 1,800 for the high-growth-rate sample, for the high-carbon and low-carbon layer respectively. Other details are described in our previous paper.<sup>20,21)</sup> The thickness of the (111) Si substrate was 1 mm. The Hall mobility was measured by the Van der Pauw method at room temperature with an indium metal ball contact. The sheet resistance was measured by the Leighton eddy current method. The X-ray diffraction was measured to examine crystal quality. During the growth, an in situ bowing monitor (Laytec) was used. A growth rate less than the maximum safe growth rate at which we can grow GaN on Si without breakage of the wafer was used. For the measurement of the bowing of the as-grown epitaxial wafer, a laser distance measurement system was used. The secondary ion mass spectrometry (SIMS) depth profile was used for the analysis of carbon concentration. The thickness of the grown layer was determined by cross-sectional scanning electron microscopy (SEM) observation.

For the growth of shallow Si-doped GaN, a multiwafer production machine of 150 mm × 7 (TAIYO NIPPON SANSO UR25k) was used.<sup>19)</sup> This reactor can also grow 100 mm × 10 wafers by using another wafer holder. Since the largest diameter of the commercial bulk GaN substrate is 100 mm, the growth condition of high-purity and high-growth-rate GaN was optimized by using the UR25k. A 50-mm-diameter bulk GaN substrate was also used to examine the effect of the dislocation in GaN on sapphire. A GaN substrate was placed at the center of the 150-mm-diameter wafer pocket so that the GaN wafer was surrounded by 6 pieces of 50 mm sapphire substrates. SiH<sub>4</sub> was used as the donor impurity. A GaN template grown on a 50-mm-diameter sapphire substrate was used for the substrate. A 50-mm-diameter bulk GaN substrate was also used for reference. The donor concentration was obtained by capacitance–voltage (C–V) measurement.

### 3. Results and discussion

#### 3.1 AlGaIn/GaN on Si

An Al<sub>0.25</sub>Ga<sub>0.75</sub>N (25 nm)/AlN (1 nm)/uid-GaN (240 nm)/carbon-doped semi-insulating (SI) GaN (1250 nm)/SLS (150 pairs, 3750 nm)/Al<sub>0.5</sub>Ga<sub>0.5</sub>N (270 nm)/AlN (150 nm)/Si structure was grown on a 200-mm-diameter (111) Si substrate. We used SLS (5 nm AlN/20 nm Al<sub>0.086</sub>Ga<sub>0.914</sub>N) structure for the compensation of the large thermal mismatch between GaN and Si substrate.<sup>22)</sup> This is our typical high-electron-mobility transistor (HEMT) structure on Si. An example of the SIMS depth profile of carbon concentration for this structure is shown in Fig. 1.<sup>23)</sup> The growth pressure was varied to adjust the carbon incorporation in each layer. For the HEMT, we need a high-purity channel region to obtain a high-electron-mobility two-dimensional electron gas (2DEG) and also to reduce the carrier trap density to eliminate current collapse.<sup>18)</sup> Beneath the 2DEG, we need a high-resistivity layer to suppress the leakage current under a

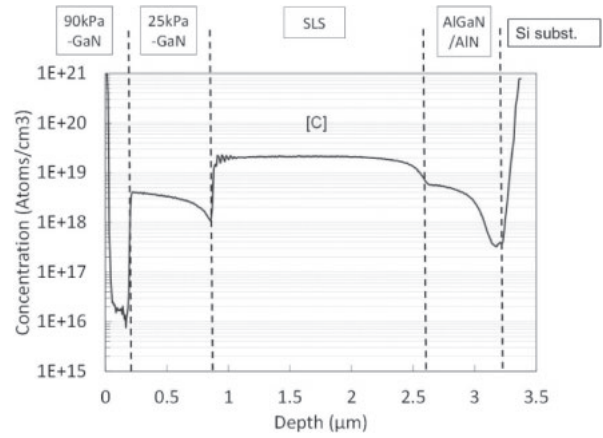


Fig. 1. Example of SIMS depth profile of carbon concentration.

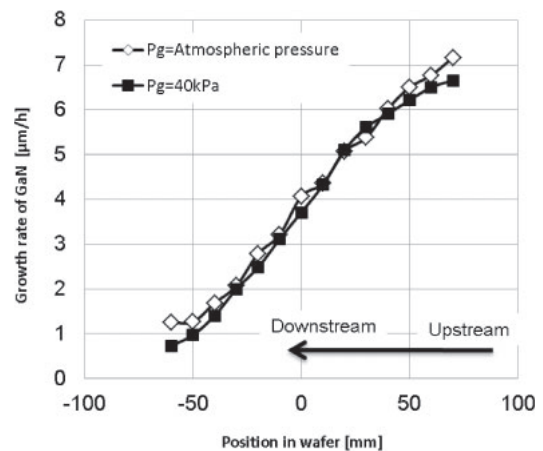


Fig. 2. Growth rate distribution of GaN along the flow direction for a stationary 150-mm-diameter sapphire substrate. Open squares show the growth rate at an atmospheric pressure, and the solid squares show the growth rate at the growth pressure ( $P_g$ ) of 40 kPa.

high applied voltage across the electrodes and ground. You can see that the carbon concentration was varied from  $10^{16}$  to  $10^{19}$  cm<sup>-3</sup> by varying the growth pressure (Fig. 1).<sup>23)</sup> The carbon concentration can be controlled by other growth parameters as follows. The carbon concentration decreases as the V/III ratio or growth temperature increases, and it increases as the growth temperature decreases.<sup>23–25)</sup> However, the order of the control range by these parameters other than growth pressure is limited. By low-temperature growth for a high carbon concentration, the surface morphology is degraded, and at a high V/III ratio for a low carbon concentration, the growth rate must be very low. Provided that the vapor phase parasitic reaction of the cluster formation is well suppressed so that the growth rate is independent of the growth pressure, the growth pressure is a very useful parameter to control the carbon concentration in a wide range from  $10^{16}$  to  $10^{19}$  cm<sup>-3</sup>.

Figure 2 shows the growth rate distribution of GaN along the flow direction for a stationary 150-mm-diameter sapphire substrate obtained by using a multiwafer machine (TAIYO NIPPON SANSO UR26k, 150 mm × 10 or 200 mm × 6). Both the atmospheric-pressure growth data and the low-pressure data at 40 kPa show good coincidence. Provided that the vapor-phase parasitic reaction of particle formation is well suppressed, the growth results at the atmospheric and

**Table I.** Growth rate of each layer for the current optimum-growth-rate sample A and high-growth-rate sample B (in  $\mu\text{m}/\text{h}$ ).

Layer	Sample A	Sample B
AlN	1.08	1.08
AlGaIn	1.20	2.40
SLS	2.00	3.46
SI-GaN	3.84	7.69
uid-GaN	2.05	2.05

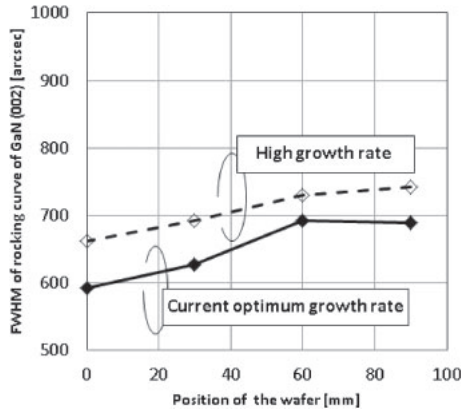


**Fig. 3.** FWHM of XRD symmetric reflection in (002) direction for both samples A and B.

low pressures should be the same, because the Reynolds number is independent of the pressure and the pressure effect of the molecular diffusion constant and the absolute concentration of precursors in vapor-phase cancel each other out. Then, we can use the growth pressure as a good parameter to control carbon incorporation in GaN and AlGaIn. In general, the growth rate of GaN is a function of growth pressure due to the cluster formation in the vapor-phase.<sup>26,27)</sup>

Next, we examined the effect of the growth rate of the SLS buffer layer on the crystal quality and 2DEG by using the same reactor, in which parasitic reactions are well suppressed as shown above. The sample structure is the same as the SIMS sample in Fig. 1. Table I shows the growth rate of each layer for the current optimum-growth-rate sample A and high-growth-rate sample B. In sample B, the compound growth rate of SLS was set to as high as  $3.46\mu\text{m}/\text{h}$ , which is 73% higher than the current optimum one. The V/III ratios of AlN and AlGaIn of SLS were 1,530 and 328, respectively. The growth rate of 5-nm-thick AlN in SLS was  $1.6\mu\text{m}/\text{h}$ . The growth rate of carbon-doped SI GaN was set as high as  $7.69\mu\text{m}/\text{h}$ . The V/III ratio was 585. To increase the growth rate, the organo-metal input flow rate was increased with a constant  $\text{NH}_3$  flow rate. The V/III ratio and growth pressure for AlN of  $1.6\mu\text{m}/\text{h}$  were substantially higher than the reported values of 250 and 5 kPa in the literature.<sup>28)</sup>

Figure 3 shows the FWHM of the X-ray rocking curve profile of (002) diffraction for both samples A and B, respectively. By increasing the growth rate, the FWHM increased from 600 to 660 arcsec in the central region. However, the amount of increase in the FWHM is within the optimization range of the growth conditions. Figure 4 shows the sheet resistance and mobility for samples A and B. The sheet resistance was increased from 280 to  $300\Omega$  by increasing the growth rate. The mobility was also decreased

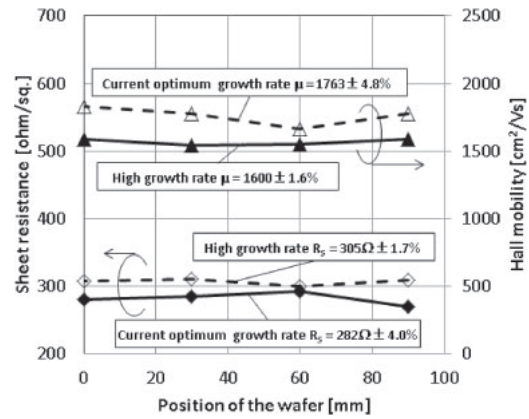


**Fig. 4.** Sheet resistance and mobility for samples A and B.

from 1,700 to  $1,600\text{cm}^2\text{V}^{-1}\text{s}^{-1}$ . These differences probably came from the roughening of the AlGaIn/AlN/GaN interface due to the high growth rate of the underlying layer, but are also within the optimization range of the growth conditions.

Another important issue is bowing control. We can control the bowing value to less than  $30\mu\text{m}$  for the current optimum growth rate condition for GaN on 1-mm-thick 200-mm-diameter Si substrate.<sup>21)</sup> However, the bowing of sample B at room temperature was concave and larger than  $80\mu\text{m}$ . To control the bowing, we may need to optimize the growth condition at the interface formation stage. In the present experiments, we can flow  $\text{NH}_3$  at a rate slightly higher than the present condition owing to the limitation of the exhaust gas abatement system. In a single-wafer reactor, however, the limitation to the process window for the growth condition would be mitigated. The above results demonstrate the possibility and challenge of increasing the growth rate of GaN on Si.

### 3.2 Requirement for the growth of GaN on GaN

Alternative, attractive device structures for GaN-based electronics are the vertical diode and transistor. The p-n diode, which offers a high-voltage operation with a low on-resistance compared with a unipolar Schottky barrier diode (SBD), is very promising for the mid-high voltage range of 1 to 3 kV. The challenges in manufacturing this device include a reduction in growth time, because the n-type GaN needs tens of microns thick and uniform silicon doping of GaN from concentrations of  $10^{15}$  to low  $10^{16}\text{cm}^{-3}$ . Producing films with low doping concentrations is not easy, requiring control of the much diluted  $\text{SiH}_4$  gas supply and a low level of carbon impurity to produce low-compensation n-type GaN.

Realising GaN films with these attributes requires a good growth process control to eliminate the parasitic reaction in the vapor-phase. It is possible to reduce the carbon concentration via atmospheric pressure growth. N-type GaN growth rates can be more than  $3\mu\text{m}/\text{h}$ , leading to runs of just several hours for epi-wafer production.<sup>25)</sup>

Figure 5 shows the carrier concentration in n-type GaN grown on 150-mm-diameter sapphire as a function of the ratio of  $\text{SiH}_4$  to trimethylgallium.<sup>19,25)</sup> At low V/III ratios, the compensation ratio of the donor is large. With increasing V/III ratio, the compensation ratio of the donor was improved (Fig. 5). For reference, Si doping was conducted for GaN on a bulk GaN substrate. The GaN on the GaN

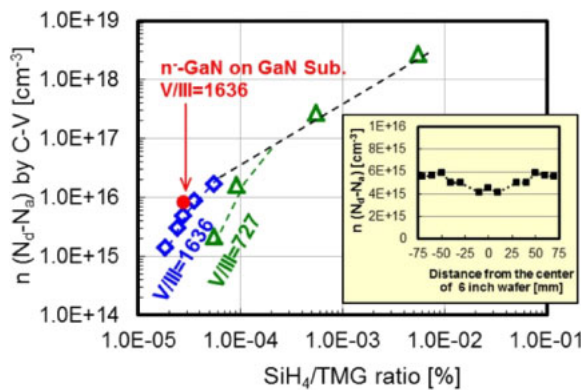


**Fig. 5.** (Color online) Carrier concentration in n-type GaN grown on 150-mm-diameter sapphire as a function of the ratio of  $\text{SiH}_4$  to trimethylgallium.<sup>19,25</sup> For reference, Si-doped GaN on a bulk GaN substrate is also shown. The inset shows the donor concentration distribution in GaN grown at  $3.6 \mu\text{m/h}$  on a 150-mm-diameter sapphire substrate.

sample showed a better donor activation, which suggests that some of the compensation effect originates from dislocations in GaN on sapphire samples. The inset in Fig. 5 shows that uniform doping at  $5 \times 10^{15} \text{cm}^{-3}$  is possible under growth rates as high as  $3.6 \mu\text{m/h}$ .

If you look at the thickness required for the vertical electron devices, you can find the necessity of in situ cleaning of the reactor to eliminate particle contamination, which is a common practice in Si LSI fabrication. To introduce an etching agent into a large-scale machine is not always easy, since we must take care of huge amounts of exhaust by-products. The divergent exhaust configuration of a multiwafer machine makes it difficult to collect the corrosive by-product of reactor cleaning. If we can increase the growth rate of GaN by a factor of ten whilst keeping a low carbon concentration, it would be easy to design an automated reactor equipped with an in situ cleaning function. As we have mentioned in introduction, the future production technology of GaN would follow the history of Si electron device fabrication. Then, the next challenge in GaN MOCVD would be high growth rate and high purity. To this end, further studies of the vapor-phase reaction control and impurity incorporation are important.

#### 4. Conclusions

The challenges in GaN MOCVD for electron device application for both GaN on Si and GaN on GaN were described. The possibility of a high growth rate for the buffer layer structure for GaN on Si was examined. In terms of XRD and electrical properties, nearly equivalent results were obtained for the layer grown at a 73% higher rate. On the other hand, the bowing was increased from less than 30 to  $80 \mu\text{m}$  for GaN on 1-mm-thick 200-mm-diameter Si substrate. These results are very promising for further increasing the growth rate of GaN on Si by using a single-wafer cluster tool, since the process window in a single-wafer cluster tool is much wider than a multiwafer large-scale reactor. However, we still need to increase the growth rate by another 73% to keep the present pace of productivity improvement of the heteroepitaxial growth.

For GaN-on-GaN application, n-GaN with a donor concentration of  $1 \times 10^{16} \text{cm}^{-3}$  was grown at a rate of  $3.7 \mu\text{m/h}$ .

The next challenge for GaN-on-GaN is to increase the growth rate by a factor of ten whilst keeping the low carbon concentration.

In conclusion, it is important to control the vapor-phase reaction to suppress the parasitic reaction for both applications.

#### Acknowledgements

The authors would like to thank the JST Super Cluster Program for partially supporting this work. We also thank Professor Takashi Egawa of Nagoya Institute of Technology for his advice on growing GaN on Si by MOCVD.

- 1) I. Akasaki and H. Amano, *Jpn. J. Appl. Phys.* **36**, 5393 (1997).
- 2) S. Nakamura, M. Senoh, and T. Mukai, *Jpn. J. Appl. Phys.* **32**, L8 (1993).
- 3) X. L. Wang, C. M. Wang, G. X. Hu, J. X. Wang, T. S. Chen, G. Jiao, J. P. Li, Y. P. Zeng, and J. M. Li, *Solid-State Electron.* **49**, 1387 (2005).
- 4) A. Chini, D. Buttari, R. Coffie, S. Heikman, S. Keller, and U. K. Mishra, *Electron. Lett.* **40**, 73 (2004).
- 5) M. Kanamura, T. Kikkawa, T. Iwai, K. Imanishi, T. Kubo, and K. Joshin, *IEDM Tech. Dig.*, 2005, p. 572.
- 6) D. Visalli, M. Van Hove, J. Derluyn, S. Degroote, M. Leys, K. Cheng, M. Germain, and G. Borghs, *Jpn. J. Appl. Phys.* **48**, 04C101 (2009).
- 7) M. Ishida, Y. Uemoto, T. Ueda, T. Tanaka, and D. Ueda, *Int. Power Electronics Conf.*, 2010, p. 1014.
- 8) S. Tripathy, V. K. X. Lin, S. B. Dolmanan, J. P. Y. Tan, R. S. Kajen, L. K. Bera, S. L. Teo, M. K. Kumar, S. Arulkumar, G. I. Ng, S. Vicknesh, S. Todd, W. Z. Wang, G. Q. Lo, H. Li, D. Lee, and S. Han, *Appl. Phys. Lett.* **101**, 082110 (2012).
- 9) D. Christy, T. Egawa, Y. Yano, H. Tokunaga, H. Shimamura, Y. Yamaoka, A. Ubukata, T. Tabuchi, and K. Matsumoto, *Appl. Phys. Express* **6**, 026501 (2013).
- 10) S. Arulkumar, G. I. Ng, S. Vicknesh, C. M. Manojkumar, M. J. Anand, H. Wang, K. S. Ang, S. L. Selvaraj, W. Z. Wang, G.-Q. Lo, and S. Tripathy, *CS MANTECH Conf.*, 2013, p. 289.
- 11) H. Nie, Q. Diduck, B. Alvarez, A. P. Edwards, B. M. Kayes, M. Zhang, G. Ye, T. Prunty, D. Bour, and I. C. Kizilyalli, *IEEE Electron Device Lett.* **35**, 939 (2014).
- 12) I. C. Kizilyalli, P. Bui-Quang, D. Disney, H. Bhatia, and O. Aktas, *Microelectron. Reliab.* **55**, 1654 (2015).
- 13) Web [<http://www.appliedmaterials.com/ja/applied-precision-5000>].
- 14) K. Matsumoto, A. Ubukata, K. Ikenaga, K. Naito, J. Yamamoto, Y. Yano, T. Tabuchi, A. Yamaguchi, Y. Ban, and K. Uchiyama, *Proc. SPIE* **8262**, 826202 (2012).
- 15) K. Matsumoto and A. Tachibana, *J. Cryst. Growth* **272**, 360 (2004).
- 16) J. R. Creighton, W. G. Breiland, M. E. Coltrin, and R. P. Pawlowski, *Appl. Phys. Lett.* **81**, 2626 (2002).
- 17) J. R. Creighton, G. T. Wang, W. G. Breiland, and M. E. Coltrin, *J. Cryst. Growth* **261**, 204 (2004).
- 18) J. Selvaraj, S. L. Selvaraj, and T. Egawa, *Jpn. J. Appl. Phys.* **48**, 121002 (2009).
- 19) K. Matsumoto, *Compd. Semicond.* **20** [3], 38 (2014).
- 20) A. Ubukata, Y. Yamaoka, A. Yamaguchi, Y. Yano, T. Tabuchi, and K. Matsumoto, *Phys. Status Solidi C* **10**, 1353 (2013).
- 21) Y. Yano, H. Tokunaga, H. Shimamura, Y. Yamaoka, A. Ubukata, T. Tabuchi, and K. Matsumoto, *Jpn. J. Appl. Phys.* **52**, 08JB06 (2013).
- 22) T. Egawa, T. Moku, H. Ishikawa, K. Ohtsuka, and T. Jimbo, *Jpn. J. Appl. Phys.* **41**, L663 (2002).
- 23) A. Ubukata, Y. Yano, H. Shimamura, A. Yamaguchi, T. Tabuchi, and K. Matsumoto, *J. Cryst. Growth* **370**, 269 (2013).
- 24) D. D. Koleske, A. E. Wickenden, R. L. Henry, and M. E. Twigg, *J. Cryst. Growth* **242**, 55 (2002).
- 25) G. Piao, K. Ikenaga, Y. Yano, H. Tokunaga, A. Mishima, Y. Ban, T. Tabuchi, and K. Matsumoto, to be submitted to *J. Cryst. Growth*.
- 26) M. Dauelsberg, D. Brien, R. Pueshe, O. Schoen, E. V. Yakovlev, A. S. Segal, and R. A. Talalaev, *J. Cryst. Growth* **315**, 224 (2011).
- 27) M. Dauelsberg, C. Martin, H. Protzmann, A. R. Boyd, E. J. Thrush, J. Kaeppler, M. Heuken, R. A. Talalaev, and A. V. Kondratyev, *J. Cryst. Growth* **298**, 418 (2007).
- 28) A. V. Lobanova, K. M. Mazaev, R. A. Talalaev, M. Leys, S. Boeykens, K. Cheng, and S. Degroote, *J. Cryst. Growth* **287**, 601 (2006).